Supplemental material

Wong et al., **https://doi.org/10.1084/jem.20181003**

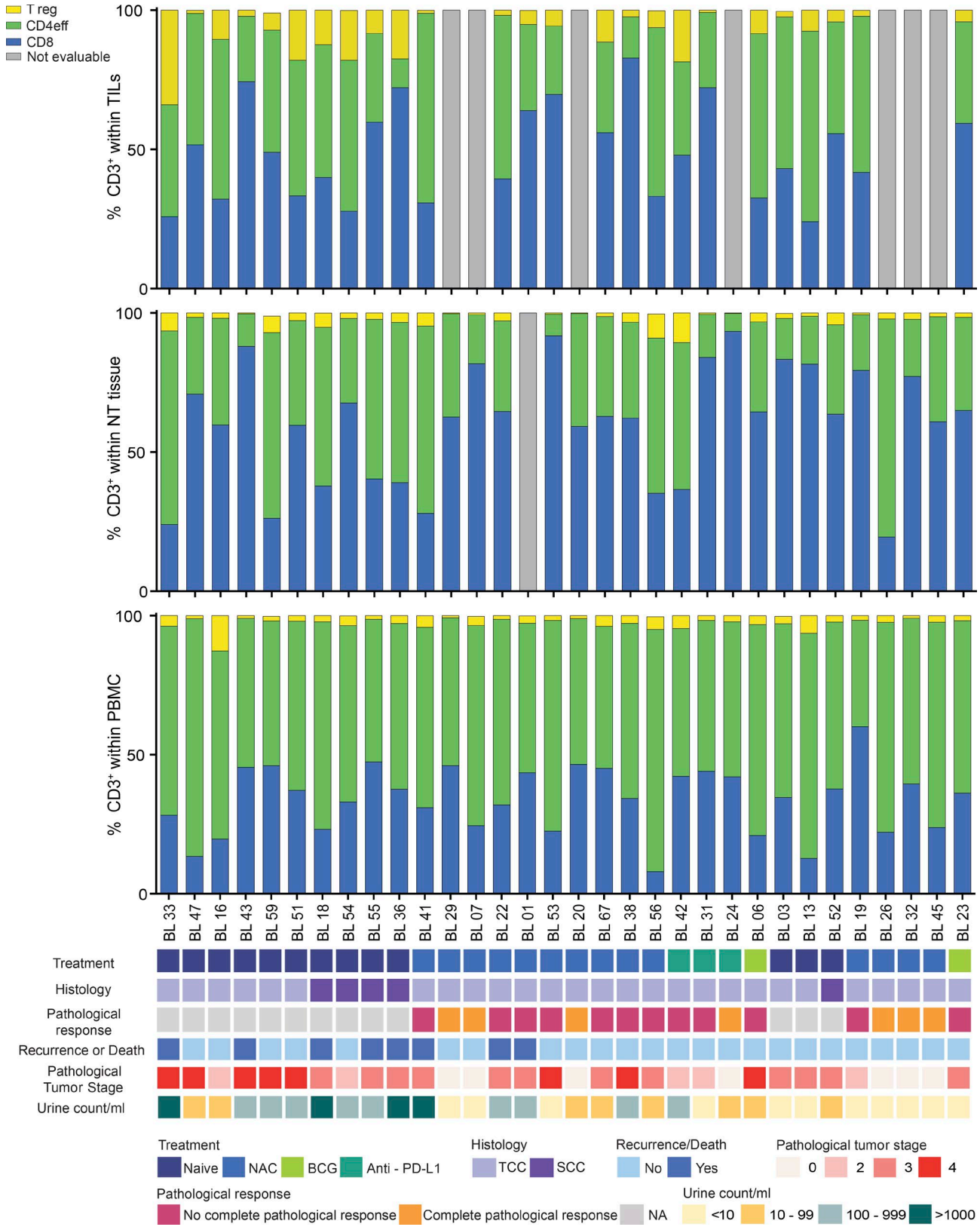

Figure S1. **Proportion of T cell subsets within CD3⁺ T lymphocytes in matched tumor, NT tissue, and peripheral blood mononuclear cells.** The proportion of CD8⁺, CD4⁺ FoxP3⁻ (CD4eff), and CD4⁺ FoxP3⁺ (T reg) cells present within the viable CD3⁺ gate in the tumor, NT tissue, and PBMC is shown. Each individual patient's prior treatment history, histological diagnosis, pathological response to therapy, clinical outcome (recurrence or death), and pathological tumor stage is shown. No pathological response is defined as having stable disease or progressive disease at time of cystectomy. Patients with a pathological response are defined as either partial or complete responders. BCG, Bacillus Calmette-Guerin; NA, not applicable; NAC, neoadjuvant chemotherapy; PD-L1, programmed death-ligand 1.

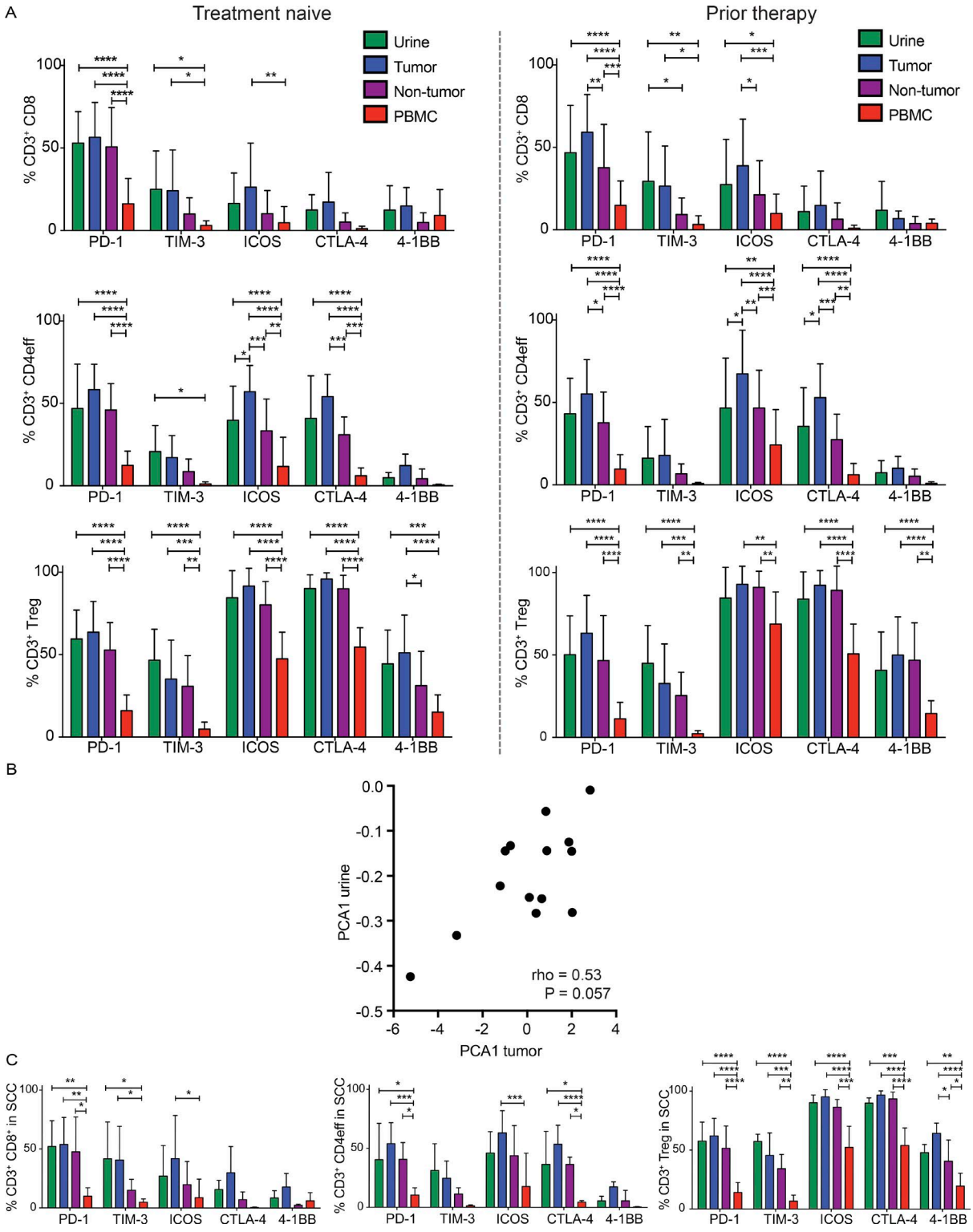

Figure S2. **UDLs exhibit a similar checkpoint landscape to tumor-infiltrating lymphocytes independent of prior therapy.** Single-level expression and coexpression of B7 and TNFR superfamily coinhibitory and costimulatory molecules on T cell subsets were quantified by flow cytometry in matched urine, tumor, NT tissue, and PBMC obtained from all patients. **(A)** Displayed is the relative expression of immune checkpoint molecules on T cell subsets within urine, tumor, NT tissue, and PBMC according to treatment history. P values were calculated using two-way ANOVA. Bars represent mean values with SD. **(B)** Displayed is a PCA using an unsupervised technique to analyze the relationship between the immune checkpoint phenotypes observed in the tumor and urine. The PCA values represent a summary of immune checkpoint frequencies for each of the T cell subsets studied in matched tumor and urine samples for each patient (n = 14). Spearman rank correlation coefficient and P values shown. **(C)** Displayed is the relative expression of T cell subset immune checkpoint molecules within urine, tumor, NT tissue, and PBMC in patients with SCC (n = 5). P values were calculated using two-way ANOVA. Bars represent mean values with SD. *, P < 0.05; **, P < 0.01; ***, P < 0.001; ****, P < 0.0001 for A and C.

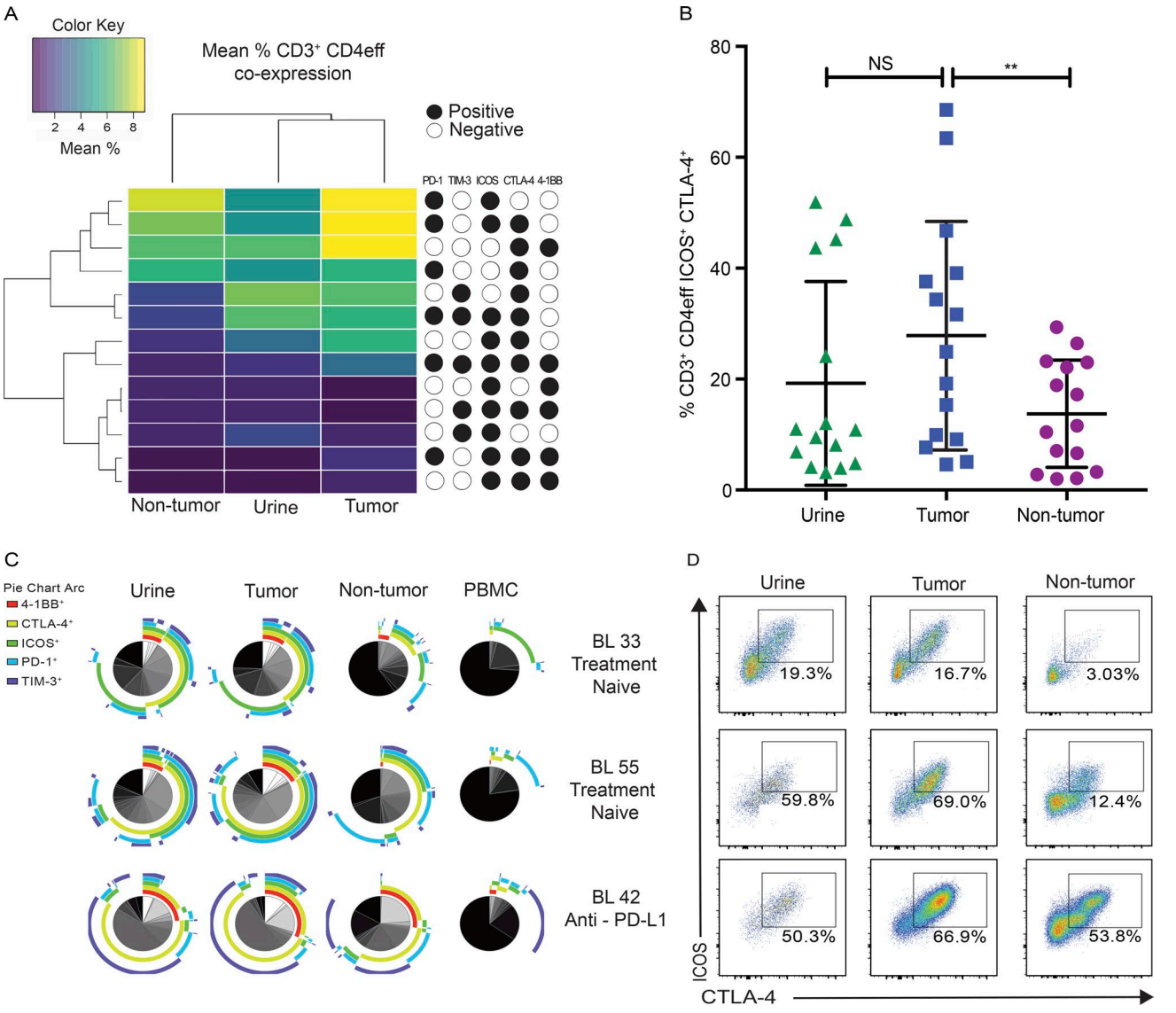

Figure S3. **CD4 effector T cells exhibit a similar coexpression checkpoint phenotype in UDLs and TILs. (A)** Displayed is a heat map showing unsupervised clustering of the mean percentage of CD4eff cells for each coexpression checkpoint phenotypes. Each row within the heat map represents a different checkpoint coexpression phenotype. The phenotype key is based on the presence (black filled circle) or absence (white circle) of each checkpoint molecule in a given phenotype. Only CD4eff coexpression phenotypes found at a frequency of ≥1% (mean across all patients) in any of tumor, urine, or NT are shown. **(B)** Graph depicts the frequency of CD4eff T cells that coexpress ICOS and CTLA-4 in tumor, urine, and NT samples. P values were calculated using paired *t* test. Bars represent mean values with SD. **, $P < 0.005$; NS, not significant. **(C)** SPICE analysis of all CD4eff T cells displaying the coexpression of checkpoint molecules in urine, tumor, NT, and PBMCs in a representative group of patients (BL 33, TCC treatment naive; BL 55, SCC treatment naive; BL 42, TCC neoadjuvant immunotherapy). Pie charts depict qualitative distribution of checkpoint expressions on CD4eff T cells. Arcs show checkpoint makeup and overlap within pie slice. **(D)** Coexpression pattern of ICOS/CTLA-4 on CD4eff on urine, tumor, and NT. Dot plots display the phenotype of CD4eff lymphocytes from matched samples from the same representative patients in C (BL 33, BL 55, and BL 42). The percentage of cells expressing each combination of checkpoint molecules is shown.

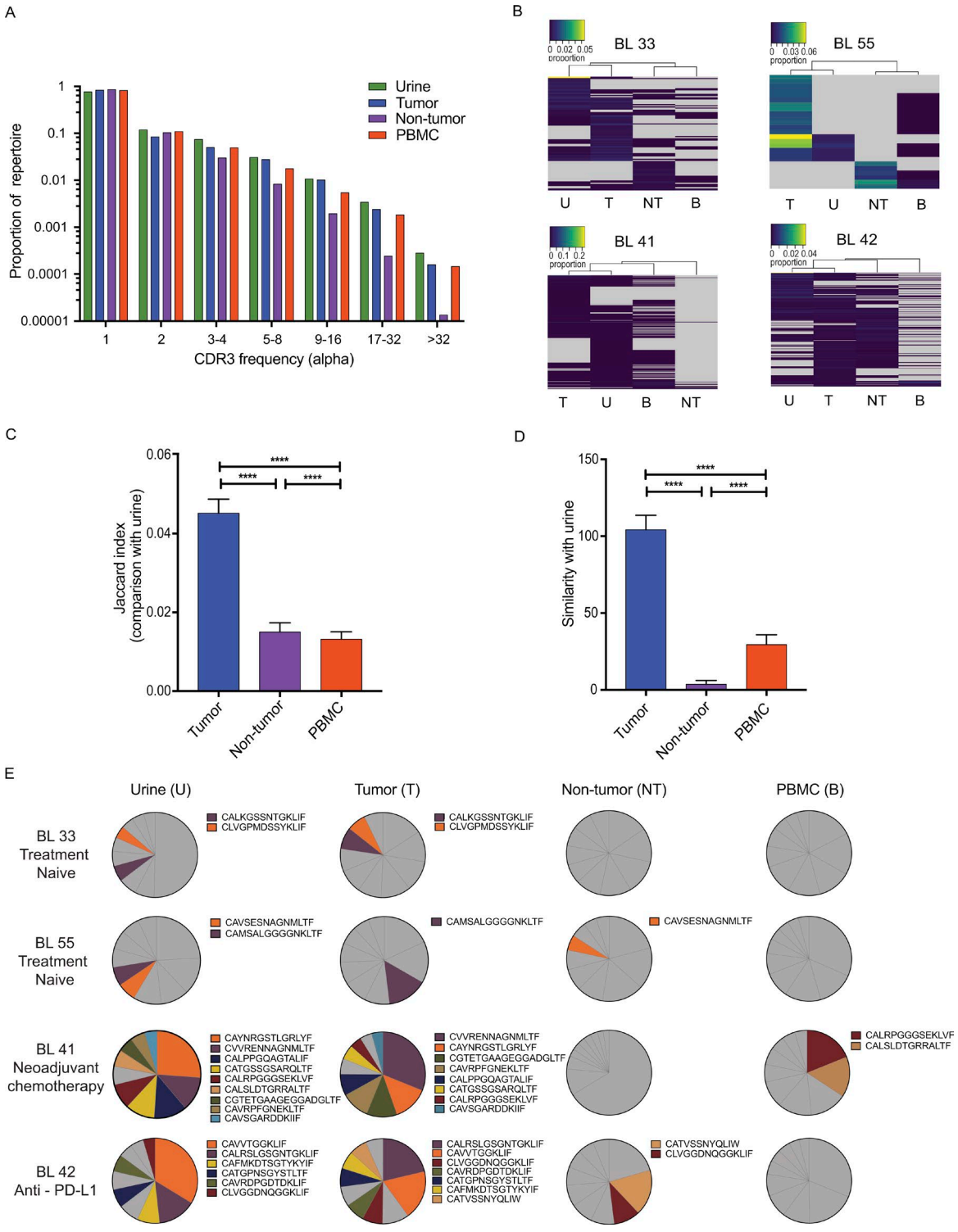

Figure S4. **The α TCR repertoire of UDLs reflects the intra-tumoral repertoire. (A)** The distribution of α chain TCRs in the urine is similar to tumor, NT tissue, and PBMCs. The proportion of TCRs found with different abundances (x axis) in urine, tumor, NT tissue, and PBMCs is shown. **(B)** Hierarchical clustering of CDR3s demonstrates similarity in the TCR repertoire of urine and tumor. CDR3s were filtered based on abundance (present at least eight times) and detected in at least one of urine, tumor, or NT tissue. Color key represents the proportion of each CDR3 within the whole repertoire. T, tumor; U, urine; B, PBMC. **(C)** The overlap, quantified by the Jaccard index, between the set of CDR3s found in urine and in each of the other compartments is shown. The results show the mean plus SD. The significance was measured by one-way ANOVA. **(D)** Similarity index (measured as the dot product of the abundances) between samples of the urine TCR repertoire and the repertoire of each other compartment. The results show the mean plus SD. The significance was measured by one-way ANOVA. **(E)** The most expanded CDR3s detected in the tumor are also expanded within the urine. Pie charts represent the 10 most abundant βCDR3s ranked in descending order in the urine, tumor, NT, and PBMCs. CDR3s among the top 10 CDR3s present in at least two of urine, tumor, NT tissue and PBMC are highlighted in color. Gray represents CDR3s that are not shared. ****, $P < 0.0001$ for C and D.

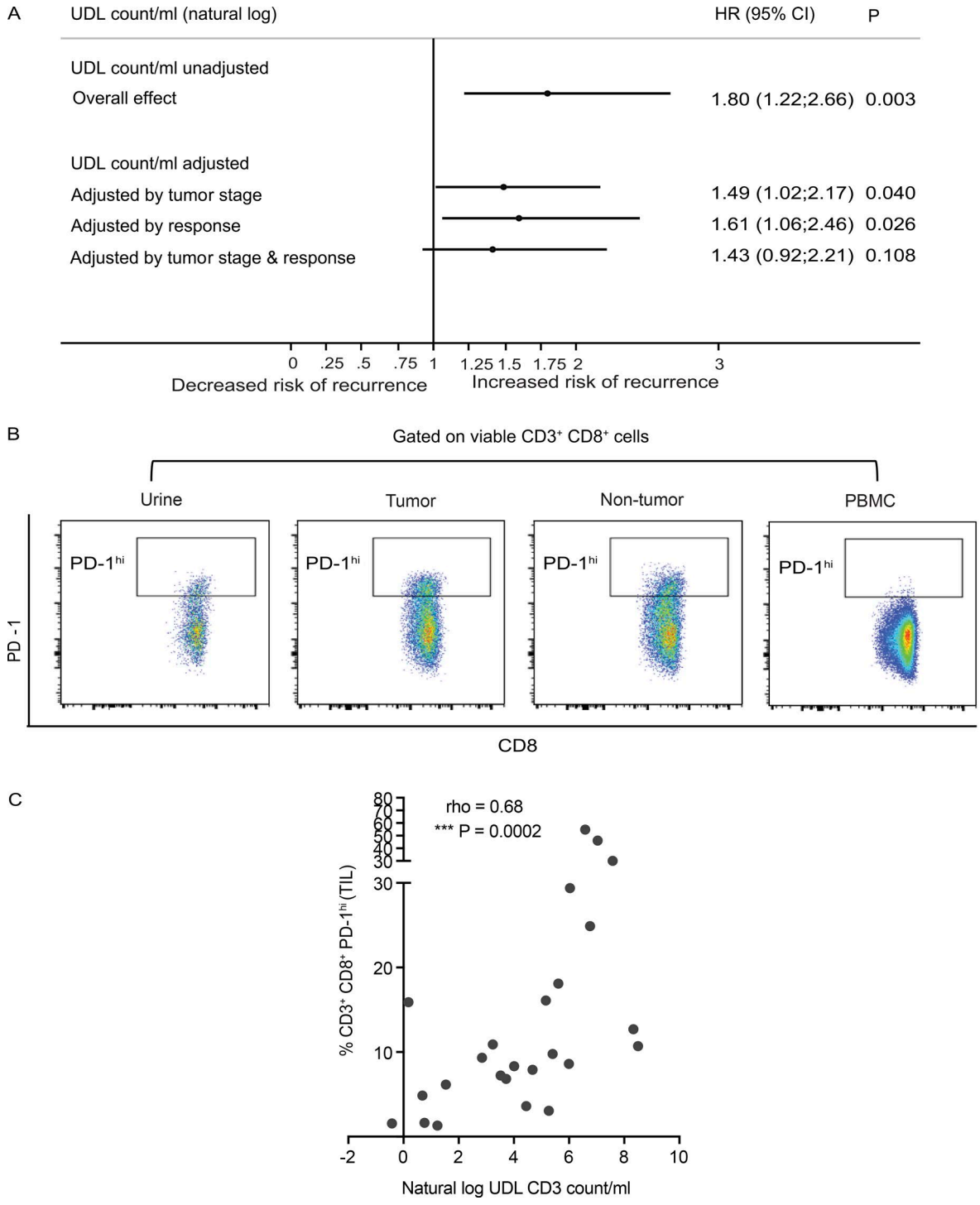

Figure S5. **Increased urinary CD3⁺CD8⁺PD-1^{hi} lymphocytes are associated with a worse clinical outcome in patients with MIBC. (A)** A forest plot using a natural log transformed UDL count/ml as a continuous variable is shown (unadjusted). A cox regression model is used with UDL count/ml adjusted for pathological tumor stage, and treatment response is demonstrated. **(B)** Multiparametric flow cytometry was used to identify CD3⁺CD8⁺PD-1^{hi} lymphocytes in the urine, tumor, NT, and PBMC samples of patients with MIBC. Dot plots and gating strategies are shown from a representative patient. CD8⁺ T cells were considered to be PD-1^{hi} with expression levels of PD-1 greater than that observed in matched PBMC samples. **(C)** Displayed is a Spearman rank correlation of the frequency of CD3⁺CD8⁺PD-1^{hi} in TIL (%) and the natural log CD3 count/ml in urine samples. Spearman rank correlation coefficient and P values shown.

Table S1. **UDL counts in age-matched patients with no known bladder pathology**

Gender	Age	Amount (ml)	Number of viable CD3	UDL count/ml
Female	28	40	8	0.20
Male	67	50	26	0.52
Male	68	40	24	0.60
Female	67	40	65	1.63
Male	49	50	134	2.68
Male	37	50	138	2.76

UDL analysis of a selected group of age-matched healthy patients being investigated for hematuria with no known bladder pathology as determined at cystoscopy. The number of viable CD3 is the number of events recorded within the viable $CD3^+$ gate on the flow cytometer. UDL count per milliliter is the number of viable CD3 per milliliter of urine collected.

Table S2. **The largest delta difference between tumor and NT checkpoint coexpression phenotypes within the effector T cells in descending order**

Phenotype	Delta between TIL and NT (%)
CD8	
PD-1/TIM-3	17.49
PD-1/ICOS	12.12
ICOS/TIM-3	11.11
PD-1/CTLA-4	9.65
CTLA-4/TIM-3	8.52
CD4eff	
CTLA-4/ICOS	13.90
CTLA-4/TIM-3	10.80
ICOS/PD-1	10.00
CTLA-4/PD-1	9.00
CTLA-4/4-1BB	7.10

Displayed are the top five coexpression phenotypes that have the highest percentage difference between tumor and non-tumor (NT) on $CD8^+$ and CD4eff T cells. The differences in the frequencies of $CD8^+$ and CD4eff T cells with each of these phenotypes are displayed in descending order.

Table S3. **Total numbers of alpha and beta CDR3s sequenced**

	Mean number of CDR3s sequenced		Range of CDR3s sequenced	
	Alpha	Beta	Alpha	Beta
Tumor	6,340	15,280	495–13,993	2,063–22,538
Urine	4,859	19,413	162–10,610	443–58,624
NT	3,579	7,200	437–7,259	1,599–15,430
PBMC	70,914	133,603	13,130–155,143	58,502–282,916

Displayed are the total numbers of alpha and beta CDR3s sequenced from tumor, urine, NT, and PBMC derived from four patients with matched available RNA. Also shown are the ranges of total numbers of alpha and beta CDR3s sequenced.